Measurement of the Inclusive Jet Cross Section using the k_T algorithm in $p\overline{p}$ Collisions at $\sqrt{s} = 1.96$ TeV

The CDF Collaboration

Draft version 2.0

We report on a measurement of the inclusive jet production cross section in $p\overline{p}$ collisions at $\sqrt{s} = 1.96$ TeV using data collected with the upgraded Collider Detector at Fermilab in Run II (CDF II) corresponding to an integrated luminosity of 385 pb^{-1}. Jets are reconstructed using the k_T algorithm. The measurement is carried out for jets with rapidity $0.1 < |y^{jet}| < 0.7$ and transverse momentum in the range $54 < p_T^{jet} < 700$ GeV/c. The measured cross section is in good agreement with next-to-leading order perturbative QCD predictions after the necessary parton-to-hadron non-perturbative corrections are included.

The measurement of the inclusive jet production in $p\overline{p}$ collisions at $\sqrt{s} = 1.96$ TeV constitutes a test of perturbative QCD (pQCD) [1] predictions over more than eight orders of magnitude in cross section, and is sensitive to the presence of physics beyond the standard model [2]. The increased center-of-mass energy and integrated luminosity in Run II at the Tevatron make it possible to measure the cross section for jets with transverse momentum [3], $\mathrm{p_T^{jet}}$, up to about 700 GeV/c, extending the $\mathrm{p_T^{jet}}$ range by more than 150 GeV/c compared with previous results [4]. This letter presents a new measurement of the inclusive jet production cross section as a function of $\mathrm{p_T^{jet}}$ for jets with $\mathrm{p_T^{jet}} > 54$ GeV/c and rapidity [3] in the region $0.1 < |\mathrm{y^{jet}}| < 0.7$, where jets are reconstructed with the $\mathrm{k_T}$ algorithm [5,6]. The measurements are corrected to the hadron level [7] and compared to parton-level pQCD next-to-leading order (NLO) predictions [8]. Similar measurements are carried out using cone-based jet algorithms in Run II [9]. However, the $\mathrm{k_T}$ algorithm has been widely used for precise QCD measurements at both e^+e^- and $e^{\pm}p$ colliders, and allows a well defined comparison to the theoretical predictions, without introducing additional parameters [6] in the calculations. A proper comparison with the theory, regardless of the jet algorithm employed, requires corrections to account for non-perturbative contributions that become important at low $\mathrm{p_T^{jet}}$. In particular, this could explain the marginal agreement observed in previous studies [10].

The CDF II detector is described in detail elsewhere [11]. Here, the sub-detectors most relevant for this analysis are briefly discussed. The detector has a charged particle tracking system immersed in a 1.4 T magnetic field, aligned coaxially with the beam line. A silicon microstrip detector provides tracking over the radial range 1.35 to 28 cm and covers the pseudorapidity [3] range $|\eta| \leq 2$. A cylindrical 3.1 m long open-cell drift chamber covers the radial range from 44 to 132 cm and provides full tracking coverage for $|\eta| \leq 1$. Segmented sampling calorimeters, arranged in a projective tower geometry, surround the tracking system and measure the energy flow of interacting particles in $|\eta| \leq 3.6$. The central barrel calorimeter [12] covers the region $|\eta| < 1$. It consists of electromagnetic and hadronic calorimeters segmented into 480 towers of size 0.1 in η and 15° in ϕ. The measured energy resolution for electrons is $\frac{\sigma(E)}{E} = \frac{13.5\%}{\sqrt{E_T\ [\mathrm{GeV}]}} \oplus 2\%$. The single-pion energy resolution, as determined from test-beam data, is $\frac{50\%}{\sqrt{E_T\ [\mathrm{GeV}]}} \oplus 3\%$. A hadronic calorimeter [13] complements the coverage of the central barrel calorimeter in the region $0.6 < |\eta| < 1.0$ and provides additional forward coverage out to $|\eta| < 1.3$. The forward region, $1.1 < |\eta| < 3.6$, is covered by new scintillator-plate electromagnetic and hadronic calorimeters. Cherenkov counters located in the $3.7 < |\eta| < 4.7$ region measure the average number of inelastic $p\overline{p}$ collisions per bunch crossing to compute the luminosity [14].

Monte Carlo event samples are used to determine the response of the detector and the correction factors to the

hadron level. The generated samples are passed through a full CDF detector simulation (based on GEANT3 [15] where the GFLASH [16] package is used to simulate the energy deposition in the calorimeters) and then reconstructed and analyzed using the same analysis chain as for the data. Samples of simulated inclusive jet events have been generated using the PYTHIA 6.203 [17] and HERWIG 6.4 [18] Monte Carlo generators. CTEQ5L [19] parton distribution functions (PDFs) are used for the proton and antiproton. The PYTHIA samples have been created using a special tuned set of parameters, denoted as PYTHIA-TUNE A, that includes enhanced contributions from initial-state gluon radiation and secondary parton interactions between proton/antiproton beam remnants. Tune A was developed with dedicated studies of the underlying event using the CDF Run I data [20], and has been shown to properly describe the measured jet shapes and energy flows in Run II [21,22]. In the case of PYTHIA, fragmentation into hadrons is carried out using the string model [23], while HERWIG implements the cluster model [24].

The $\mathrm{k_T}$ algorithm is used to reconstruct jets from the energy depositions in the calorimeter towers with transverse momentum above 0.1 GeV/c. First, all towers are considered as protojets. The quantities $\mathrm{k_{T,i}} = \mathrm{P^2_{T,i}}$ and $\mathrm{k_{T,(i,j)}} = \min(\mathrm{P^2_{T,i}}, \mathrm{P^2_{T,j}}) \cdot \Delta\mathrm{R^2_{i,j}}/\mathrm{D^2}$, are computed for each protojet and pair of protojets respectively, where $\mathrm{P_{T,i}}$ denotes the transverse momentum of the $\mathrm{i^{th}}$ protojet, $\Delta R_{\mathrm{i,j}}$ is the distance ($y - \phi$ space) between each pair of protojets, and D is a parameter that approximately controls the size of the jet. All $\mathrm{k_{T,i}}$ and $\mathrm{k_{T,(i,j)}}$ values are then collected into a single sorted list. In this combined sorted list, if the smallest quantity is of the type $\mathrm{k_{T,i}}$ the corresponding protojet is promoted to be a jet and removed from the list. Otherwise, if the smallest quantity is of the type $\mathrm{k_{T,(i,j)}}$, the protojets are combined into a single protojet by summing up their four-vector components. The procedure is iterated over protojets until the list is empty. The jet transverse momentum, rapidity, and azimuthal angle, as determined using the calorimeter towers, are denoted as $\mathrm{p^{jet}_{T,CAL}}$, $\mathrm{y^{jet}_{CAL}}$, and $\phi^{\mathrm{jet}}_{\mathrm{CAL}}$, respectively. The same jet algorithm is applied to all the final-state particles in Monte Carlo generated events to search for jets at the hadron level. The resulting hadron-level jet variables are denoted as $\mathrm{p^{jet}_{T,HAD}}$, $\mathrm{y^{jet}_{HAD}}$, and $\phi^{\mathrm{jet}}_{\mathrm{HAD}}$.

The measurements presented in this letter correspond to a total integrated luminosity of 385 ± 22 pb^{-1}. Events are selected *online* using three-level trigger paths [25]. In the first-level trigger, a single trigger tower with E_T above 5 GeV or 10 GeV is required. In the second-level trigger, clusters are formed around the selected trigger towers, and a cluster with E_T above 15 to 90 GeV, depending on the trigger path, is required. In the third-level trigger, jets are reconstructed using a cone-based algorithm, and a jet with E_T above 20 to 100 GeV is required. Jets are then searched for using the $\mathrm{k_T}$ algorithm, as explained above, with $D = 0.7$. For each trigger data sample, the threshold

on the minimum $\mathrm{p}_{\mathrm{T,CAL}}^{\mathrm{jet}}$ is chosen in such a way that the trigger selection is fully efficient. The events are required to have at least one jet with rapidity in the region $0.1 < |\mathrm{y}_{\mathrm{CAL}}^{\mathrm{jet}}| < 0.7$ and corrected transverse momentum (see below) above 54 GeV/c. The events are selected to have at least one reconstructed primary vertex with z-position within 60 cm around the nominal interaction point. In order to remove beam-related backgrounds and cosmics rays, the events are required to fulfill $\not\!\!E_T/\sqrt{\Sigma E_T} < F(\mathrm{p}_{\mathrm{T,CAL}}^{\mathrm{leading\ jet}})$, where $\not\!\!E_T$ denotes the missing transverse energy [26] and $\Sigma E_T = \sum_i E_T^i$ is the total transverse energy of the event, as measured using calorimeter towers with E_T above 100 MeV. The threshold function $F(\mathrm{p}_{\mathrm{T,CAL}}^{\mathrm{leading\ jet}})$ is defined as $F(\mathrm{p}_{\mathrm{T}}^{\mathrm{jet}}) = \min(2 + 0.0125 \times \mathrm{p}_{\mathrm{T}}^{\mathrm{jet}}, 7)$, where $\mathrm{p}_{\mathrm{T,CAL}}^{\mathrm{leading\ jet}}$ is the uncorrected transverse momentum of the leading jet (highest $\mathrm{p}_{\mathrm{T}}^{\mathrm{jet}}$) and the units are GeV. This criterion is designed to preserve more than 95% of the QCD events, as determined from Monte Carlo studies. A visual scan of the events with $\mathrm{p}_{\mathrm{T,CAL}}^{\mathrm{jet}}$ above 400 GeV/c showed no remaining backgrounds.

The measured jet transverse momentum includes additional contributions from multiple proton-antiproton interactions per bunch crossing at high instantaneous luminosity. This mainly affects the measured cross section at low $\mathrm{p}_{\mathrm{T}}^{\mathrm{jet}}$ where the contributions are sizeable. The data used for this measurement were collected at Tevatron instantaneous luminosities varying between $0.2 \times 10^{31}\mathrm{cm}^{-2}\mathrm{s}^{-1}$ and $9.6 \times 10^{31}\mathrm{cm}^{-2}\mathrm{s}^{-1}$. The average instantaneous luminosity was $2.6 \times 10^{31}\mathrm{cm}^{-2}\mathrm{s}^{-1}$, which corresponds to less than one interaction per bunch crossing. At the highest instantaneous luminosities, an average of two interactions per bunch crossing are produced. In CDF, multiple interactions are identified via the presence of additional primary vertices reconstructed from charged particles. The measured jet transverse momenta are corrected for this effect by removing a certain amount of transverse momentum, ϵ, for each additional primary vertex observed in the event. A value $\epsilon = 1.62^{+0.70}_{-0.46}$ GeV/c is determined from the data by requiring that, after the correction is applied, the ratio of cross sections at low and high instantaneous luminosities does not show any $\mathrm{p}_{\mathrm{T}}^{\mathrm{jet}}$ dependence.

The reconstruction of the jet variables in the calorimeter is studied using matched pairs of jets ($y - \phi$ space) at the calorimeter and hadron levels in the Monte Carlo. These studies indicate that the angular variables of a jet are reconstructed with no significant systematic shift and with a resolution better than 0.05 units in y and ϕ at low $\mathrm{p}_{\mathrm{T,CAL}}^{\mathrm{jet}}$, improving as $\mathrm{p}_{\mathrm{T,CAL}}^{\mathrm{jet}}$ increases. The measured jet transverse momentum systematically underestimates that of the hadron level jet, which is mainly attributed to the non-compensating nature of the calorimeter [27]. For jets with $\mathrm{p}_{\mathrm{T,CAL}}^{\mathrm{jet}}$ about 50 GeV/c, the jet transverse momentum is reconstructed with an average shift of -19% and a resolution of 14%. The jet reconstruction improves as $\mathrm{p}_{\mathrm{T,CAL}}^{\mathrm{jet}}$ increases. For jets with $\mathrm{p}_{\mathrm{T,CAL}}^{\mathrm{jet}}$ about 500 GeV/c, the

average shift is -5% and the resolution is about 7%. In order to evaluate how well the Monte Carlo reproduces the measured jet energy resolutions, the bisector method [28] is employed. Data and Monte Carlo agree within a relative uncertainty of $\pm 8\%$ over the whole $\mathrm{p_{T,CAL}^{jet}}$ range.

The measured $\mathrm{p_{T,CAL}^{jet}}$ distribution is corrected to the hadron level using Monte Carlo event samples. PYTHIA-TUNE A provides a reasonable description of the different jet and underlying event quantities, and is used to determine the correction factors in the unfolding procedure. In order to avoid any bias on the correction factors due to the particular PDF set used, which translates into slightly different simulated $\mathrm{p_{T,CAL}^{jet}}$ distributions, PYTHIA-TUNE A is re-weighted until it accurately follows the measured $\mathrm{p_{T,CAL}^{jet}}$ spectrum. The unfolding is carried out in two steps. First, an average correction is computed using matched pairs of jets at the calorimeter and hadron levels. The correlation $< \mathrm{p_{T,HAD}^{jet}} - \mathrm{p_{T,CAL}^{jet}} >$ vs $< \mathrm{p_{T,CAL}^{jet}} >$ is used to extract multiplicative correction factors which are then applied to the measured jets to obtain the corrected transverse momenta, $\mathrm{p_{T,COR}^{jet}}$. A raw cross section is defined in bins of $\mathrm{p_{T,COR}^{jet}}$ as $\frac{\mathrm{d}^2\sigma}{\mathrm{dp_{T,COR}^{jet}dy_{CAL}^{jet}}} = \frac{1}{\mathcal{L}} \frac{N_{\mathrm{COR}}^{\mathrm{jet}}}{\Delta \mathrm{p_{T,COR}^{jet}}\ \Delta \mathrm{y_{CAL}^{jet}}}$, where $N_{\mathrm{COR}}^{\mathrm{jet}}$ denotes the total number of jets measured in a given $\mathrm{p_{T,COR}^{jet}}$ bin, $\Delta \mathrm{p_{T,COR}^{jet}}$ is the size of the bin, $\Delta \mathrm{y_{CAL}^{jet}}$ denotes the region in $\mathrm{y_{CAL}^{jet}}$ considered, and $\mathcal{L}$ is the total luminosity of the data sample. Second, the measurements are corrected for acceptance and smearing effects to the hadron level using a bin-by-bin unfolding procedure, which also accounts for the efficiency of the selection criteria. The unfolding factors, $U(\mathrm{p_{T,COR}^{jet}}) = \frac{\mathrm{d}^2\sigma/\mathrm{dp_{T,HAD}^{jet}dy_{HAD}^{jet}}}{\mathrm{d}^2\sigma/\mathrm{dp_{T,COR}^{jet}dy_{CAL}^{jet}}}$, are extracted from Monte Carlo and applied to the measured $\mathrm{p_{T,COR}^{jet}}$ distribution to obtain the final result. The factor $U(\mathrm{p_{T,COR}^{jet}})$ increases with $\mathrm{p_{T,COR}^{jet}}$ and varies between 1.04 at low $\mathrm{p_{T,COR}^{jet}}$ and 1.3 at very high $\mathrm{p_{T,COR}^{jet}}$.

A detailed study of the different systematic uncertainties was carried out [29]. The measured jet energies were varied by $\pm 2\%$ at low $\mathrm{p_T^{jet}}$ and $\pm 3\%$ at high $\mathrm{p_T^{jet}}$ to account for the uncertainty on the absolute energy scale in the calorimeter [30]. This introduces an uncertainty on the final measurement which varies between $\pm 10\%$ at low $\mathrm{p_T^{jet}}$ and $^{+55\%}_{-40\%}$ at high $\mathrm{p_T^{jet}}$. A $\pm 8\%$ uncertainty on the jet energy resolution introduces an uncertainty in the measured cross section between $\pm 2\%$ at low $\mathrm{p_T^{jet}}$ and $\pm 8\%$ at high $\mathrm{p_T^{jet}}$. The unfolding procedure was repeated using HERWIG instead of PYTHIA-TUNE A to account for the uncertainty on the modeling of the parton cascades and the jet fragmentation into hadrons. This translates into an uncertainty about $\pm 5\%$ at low $\mathrm{p_T^{jet}}$. The unfolding procedure was also carried out using unweighted PYTHIA-TUNE A, to estimate the residual dependence on the $\mathrm{p_T^{jet}}$ spectrum. This introduces an uncertainty of $\pm 4\%$ above 400 GeV/c, which becomes negligible at lower $\mathrm{p_T^{jet}}$. The quoted uncertainty on ϵ was taken into account. The effect on the measured cross section is less than $\pm 3\%$ and negligible for jets with $\mathrm{p_T^{jet}}$ above

200 GeV/c. Other sources of systematic uncertainties were found to contribute less than 1% to the total systematic uncertainty. An additional 5.8% uncertainty on the total luminosity is not included in the following Figures and Table.

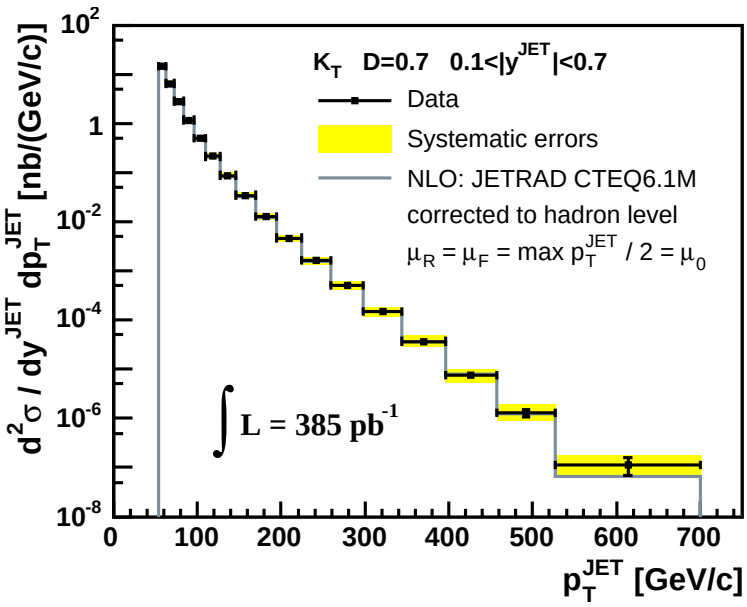

FIG. 1. Measured inclusive jet cross section (black dots) as a function of p_T^{jet} compared to NLO pQCD predictions (histogram). The shaded band shows the total systematic uncertainty on the measurement.

Figure 1 shows the measured cross section as a function of p_T^{jet} compared to NLO pQCD predictions. The data are reported in Table I. The cross section decreases by more than eight orders of magnitude as p_T^{jet} increases from 54 GeV/c up to about 700 GeV/c. The NLO pQCD predictions are computed using the JETRAD program [8] with CTEQ6.1M PDFs [31] and the renormalization and factorization scales (μ_R and μ_F) set to $\mu_0 = \max\,(p_T^{jet})/2$.

Different sources of uncertainty in the theoretical predictions were considered. The main contribution comes from the uncertainty on the PDFs and was computed using the Hessian method [32]. It varies from $^{+20\%}_{-10\%}$ at low p_T^{jet}, and $^{+7\%}_{-5\%}$ for p_T^{jet} about 100 GeV/c, to $^{+70\%}_{-30\%}$ at high p_T^{jet}, dominated by the limited knowledge of the gluon PDF. An increase of μ_R and μ_F from μ_0 to $2\mu_0$ reduces the theoretical predictions by 2% at low p_T^{jet} and 8% at high p_T^{jet}. Values significantly smaller than μ_0 lead to unstable NLO results and were not considered.

The theoretical prediction includes a correction factor, $C_{\rm HAD}(p_T^{jet})$, that approximately accounts for non-perturbative contributions from the underlying event and fragmentation into hadrons, which are not present in the pQCD calculation (see Table I). $C_{\rm HAD}(p_T^{jet})$ was estimated, using PYTHIA-TUNE A, as the ratio between the nominal $p_{T,\rm HAD}^{jet}$ distribution and the one obtained by turning off the interactions between proton and antiproton remnants and

the string fragmentation in the Monte Carlo. The parton-to-hadron correction shows a strong p_T^{jet} dependence and decreases as p_T^{jet} increases from about 1.2 at p_T^{jet} of 54 GeV/c, and 1.1 for p_T^{jet} about 100 GeV/c, to 1.02 at high p_T^{jet}. The uncertainty on $C_{HAD}(p_T^{jet})$ is about 13% at low p_T^{jet} and decreases up to 1.6% at high p_T^{jet}, as determined from the difference between the parton-to-hadron correction factors obtained using HERWIG instead of PYTHIA-TUNE A.

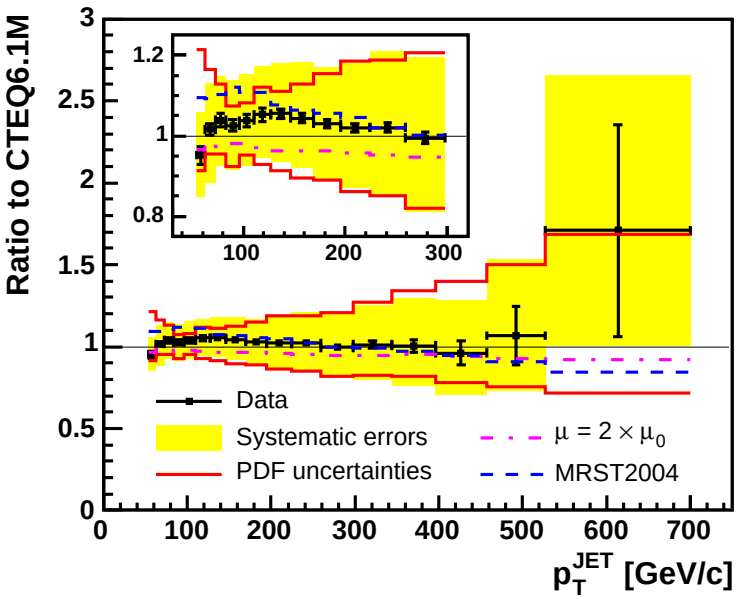

FIG. 2. Ratio Data/Theory as a function of p_T^{jet}. The inclosed figure expands the region $p_T^{jet} < 298$ GeV/c. The error bars (shaded band) show the total statistical (systematic) uncertainty on the data. A 5.8% uncertainty on the luminosity is not included. The solid lines indicate the PDF uncertainty on the theoretical prediction. The dashed line presents the ratio of MRST2004 and CTEQ6.1M predictions. The dotted-dashed line shows the ratio of CTEQ6.1M predictions with $\mu_{R,F}$ set to $2\mu_0$ and μ_0.

Figure 2 shows the ratio data/theory as a function of p_T^{jet}. Good agreement is observed between the measured cross section and the theoretical predictions. In particular, no significant deviation from the pQCD prediction is observed at high p_T^{jet}. A χ^2 test, where all the systematic uncertainties on the data are considered independent but fully correlated across different p_T^{jet} bins and the uncertainty on C_{HAD} is also included, gives a χ^2 probability of 56%. In addition, Figure 2 shows the ratio between pQCD predictions using MRST2004 [33] and CTEQ6.1M PDF sets. This changes the pQCD prediction by +10% at low p_T^{jet} and −15% at high p_T^{jet}, well inside the theoretical and experimental uncertainties.

The complete analysis was repeated using different values for the D parameter in the k_T algorithm ($D = 0.5$ and $D = 1.0$) [29]. In both cases, good agreement was again observed between the measured cross sections and the NLO

pQCD predictions in the whole range in p_T^{jet}. As the D parameter decreases, the measurement becomes less sensitive to the presence and proper modeling of the non-perturbative underlying event contributions. For $D = 0.5$ ($D = 1.0$) a parton-to-hadron correction factor $C_{HAD} = 1.1$ ($C_{HAD} = 1.4$) is applied at low p_T^{jet}. This validates the experimental procedure followed to determine the cross section and demonstrates a good control of the parton-to-hadron correction factors applied to the pQCD predictions.

p_T^{jet} [GeV/c]	$\frac{d^2\sigma}{dp_T^{jet}dy^{jet}} \pm$ (stat.) $\pm$ (sys.) [nb/(GeV/c)]	$C_{HAD} \pm$ (stat.) $\pm$ (sys.) parton $\rightarrow$ hadron
54 - 62	$(14.6 \pm 0.2^{+1.6}_{-1.6}) \times 10^{0}$	$1.202 \pm 0.013 \pm 0.158$
62 - 72	$(6.53 \pm 0.04^{+0.75}_{-0.84}) \times 10^{0}$	$1.154 \pm 0.003 \pm 0.113$
72 - 83	$(2.81 \pm 0.02^{+0.30}_{-0.30}) \times 10^{0}$	$1.134 \pm 0.005 \pm 0.094$
83 - 96	$(1.18 \pm 0.01^{+0.13}_{-0.12}) \times 10^{0}$	$1.113 \pm 0.006 \pm 0.077$
96 - 110	$(5.04 \pm 0.04^{+0.56}_{-0.54}) \times 10^{-1}$	$1.098 \pm 0.004 \pm 0.066$
110 - 127	$(2.15 \pm 0.02^{+0.25}_{-0.22}) \times 10^{-1}$	$1.079 \pm 0.005 \pm 0.047$
127 - 146	$(8.81 \pm 0.05^{+1.04}_{-0.98}) \times 10^{-2}$	$1.064 \pm 0.003 \pm 0.037$
146 - 169	$(3.45 \pm 0.02^{+0.46}_{-0.41}) \times 10^{-2}$	$1.057 \pm 0.004 \pm 0.030$
169 - 195	$(1.28 \pm 0.01^{+0.17}_{-0.17}) \times 10^{-2}$	$1.047 \pm 0.003 \pm 0.023$
195 - 224	$(4.67 \pm 0.02^{+0.74}_{-0.68}) \times 10^{-3}$	$1.043 \pm 0.003 \pm 0.018$
224 - 259	$(1.63 \pm 0.01^{+0.30}_{-0.27}) \times 10^{-3}$	$1.039 \pm 0.004 \pm 0.015$
259 - 298	$(5.08 \pm 0.06^{+1.02}_{-0.93}) \times 10^{-4}$	$1.034 \pm 0.003 \pm 0.010$
298 - 344	$(1.50 \pm 0.03^{+0.36}_{-0.31}) \times 10^{-4}$	$1.030 \pm 0.005 \pm 0.008$
344 - 396	$(3.70 \pm 0.14^{+1.07}_{-0.89}) \times 10^{-5}$	$1.016 \pm 0.009 \pm 0.006$
396 - 457	$(7.50 \pm 0.55^{+2.52}_{-2.01}) \times 10^{-6}$	$1.017 \pm 0.018 \pm 0.009$
457 - 527	$(1.31 \pm 0.22^{+0.57}_{-0.42}) \times 10^{-6}$	$1.009 \pm 0.003 \pm 0.019$
527 - 700	$(1.14 \pm 0.43^{+0.63}_{-0.47}) \times 10^{-7}$	$1.018 \pm 0.002 \pm 0.016$

TABLE I. Measured inclusive jet differential cross section as a function of p_T^{jet}. An additional 5.8% uncertainty on the luminosity is not included. The parton-to-hadron correction factors, $C_{HAD}(p_T^{jet})$, are applied to the pQCD predictions.

In summary, we have presented results on inclusive jet production in $p\overline{p}$ collisions at $\sqrt{s} = 1.96$ TeV using the k_T algorithm, for jets with transverse momentum $p_T^{jet} > 54$ GeV/c and jet rapidity in the region $0.1 < |y^{jet}| < 0.7$, based on 385 pb^{-1} of CDF Run II data. The measured cross section is in agreement with NLO pQCD predictions after the necessary parton-to-hadron non-perturbative corrections are taken into account.

Acknowledgments

We thank the Fermilab staff and the technical staffs of the participating institutions for their vital contributions. This work was supported by the U.S. Department of Energy and National Science Foundation; the Italian Istituto Nazionale di Fisica Nucleare; the Ministry of Education, Culture, Sports, Science and Technology of Japan; the

Natural Sciences and Engineering Research Council of Canada; the National Science Council of the Republic of China; the Swiss National Science Foundation; the A.P. Sloan Foundation; the Bundesministerium fuer Bildung und Forschung, Germany; the Korean Science and Engineering Foundation and the Korean Research Foundation; the Particle Physics and Astronomy Research Council and the Royal Society, UK; the Russian Foundation for Basic Research; the Comision Interministerial de Ciencia y Tecnologia, Spain; in part by the European Community's Human Potential Programme under contract HPRN-CT-2002-00292; and the Academy of Finland.

---

[1] D.J. Gross and F. Wilczek, Phys. Rev. D **8**, 3633 (1973).

[2] D. Stump et al., JHEP **0310**, 046 (2003).

[3] We use a cylindrical coordinate system about the beam axis in which θ is the polar angle and ϕ is the azimuthal angle. We define $E_T = E\ \sin\theta$ and $p_T = p\ \sin\theta$ where E is energy measured in calorimeter towers considered to be massless. The pseudorapidity is defined as $\eta = -\ln(\tan(\frac{\theta}{2}))$ and the rapidity as $y = \frac{1}{2}\ln(\frac{\mathrm{E+p_z}}{\mathrm{E-p_z}})$.

[4] T. Affolder *et al.* (CDF Collaboration), Phys. Rev. D **64**, 032001 (2001). [Erratum-ibid. D **65**, 039903 (2002)].
B. Abbott *et al.* (DØ Collaboration), Phys. Rev. Lett. **82**, 2451 (1999).

[5] S. Catani, Yu.L. Dokshitser, M.H. Seymour and B.R. Webber, Nucl. Phys. B **406**, 187 (1993).

[6] S.D. Ellis and D.E. Soper, Phys. Rev. D **48**, 3160 (1993).

[7] The hadron level in the Monte Carlo generators is defined using particles with lifetime above 10^{-11}s.

[8] W.T. Giele, E.W.N. Glover and David A. Kosower, Nucl. Phys. B **403**, 633 (1993).

[9] A. Abulencia *et al.* (CDF Collaboration), in preparation.

[10] V.M. Abazov *et al.* (DØ Collaboration), Phys. Lett. B **525**, 211 (2002).

[11] D. Acosta *et al.* (CDF Collaboration), Phys. Rev. D **71**, 032001 (2005).

[12] L. Balka *et al.*, Nucl. Instrum. Meth. A **267**, 272 (1988).

[13] S. Bertolucci *et al.*, Nucl. Instrum. Meth. A **267**, 301 (1988).

[14] D. Acosta *et al.*, Nucl. Instrum. Meth., A **494**, 57 (2002).

[15] R. Brun *et al.*, Tech. Rep. CERN-DD/EE/84-1, 1987.

[16] G. Grindhammer, M. Rudowicz and S. Peters, Nucl. Instrum. Meth. A **290**, 469 (1990).

[17] T. Sjöstrand *et al.*, Comp. Phys. Comm. **135**, 238 (2001).

[18] G. Corcella *et al.*, JHEP **0101**, 010 (2001).

[19] H.L. Lai *et al.*, Eur. Phys. J. C **12**, 375 (2000).

[20] T. Affolder *et al.* (CDF Collaboration), Phys. Rev. D **65**, 092002 (2002).

[21] D. Acosta *et al.* (CDF Collaboration), Phys. Rev. D **71**, 112002 (2005).

[22] V.M. Abazov *et al.* (DØ Collaboration), Phys. Rev. Lett. **94**, 221801 (2005).

[23] B. Andersson *et al.*, Phys. Rep. **97**, 31 (1983).

[24] B.R. Webber, Nucl. Phys. B **238**, 492 (1984).

[25] B. L. Winer, Int. J. Mod. Phys. A **16S1C**, 1169 (2001).

[26] $\not{E}_T$ is defined as the norm of $-\sum_i E_T^i \cdot \vec{n}_i$, where $\vec{n}_i$ is the unit vector in the azimuthal plane that points from the beamline to the i-th calorimeter tower.

[27] S.R. Hahn *et al.*, Nucl. Instrum. Meth. A **267**, 351 (1988).

[28] P. Bagnaia *et al.* (UA2 Collaboration), Phys. Lett. B **144**, 283 (1984).

[29] Olga Norniella, PhD. Thesis, University of Barcelona.

[30] J.Adelman *et al.*, hep-ex/0510047.

[31] J. Pumplin *et al.*, JHEP **0207**, 012 (2002).

[32] J. Pumplin *et al.*, Phys. Rev. D **65**, 014013 (2002).

[33] A. D. Martin, R.G. Roberts, W. J. Stirling, R. S. Thorne, Eur. Phys. J. C **23**, 73 (2002).